

Polarized neutron reflectometry study of depth dependent magnetization variation in Co thin film due to strain transfer from PMN-PT substrate

Cite as: J. Appl. Phys. **124**, 113903 (2018); <https://doi.org/10.1063/1.5037601>

Submitted: 25 April 2018 . Accepted: 19 August 2018 . Published Online: 21 September 2018

Md Mamun Al-Rashid, Dhritiman Bhattacharya, Alexander Grutter , Brian Kirby, and Jayasimha Atulasimha



View Online



Export Citation



CrossMark

ARTICLES YOU MAY BE INTERESTED IN

[Reversible electrical-field control of magnetization and anomalous Hall effect in Co/PMN-PT hybrid heterostructures](#)

Applied Physics Letters **112**, 152904 (2018); <https://doi.org/10.1063/1.5022381>

[Perspective: Magnetoelectric switching in thin film multiferroic heterostructures](#)

Journal of Applied Physics **123**, 240901 (2018); <https://doi.org/10.1063/1.5031446>

[Reversible and magnetically unassisted voltage-driven switching of magnetization in FeRh/PMN-PT](#)

Applied Physics Letters **113**, 152901 (2018); <https://doi.org/10.1063/1.5040184>

Journal of
Applied Physics

SPECIAL TOPIC:
Polymer-Grafted Nanoparticles

Submit Today!

Polarized neutron reflectometry study of depth dependent magnetization variation in Co thin film due to strain transfer from PMN-PT substrate

Md Mamun Al-Rashid,^{1,2,a)} Dhritiman Bhattacharya,^{1,a)} Alexander Grutter,^{3,a)} Brian Kirby,^{3,a)} and Jayasimha Atulasimha^{1,2,a)}

¹Mechanical and Nuclear Engineering, Virginia Commonwealth University, Richmond, Virginia 23284, USA

²Electrical and Computer Engineering, Virginia Commonwealth University, Richmond, Virginia 23284, USA

³NIST Center for Neutron Research, NIST, Gaithersburg, Maryland 20899, USA

(Received 25 April 2018; accepted 19 August 2018; published online 21 September 2018)

We studied the depth dependent magnetization profile of the magnetostrictive Co thin film layer in a $(\text{PbMg}_{0.33}\text{Nb}_{0.67})_{1-x}:(\text{PbTiO}_3)_x$ (PMN-PT) (011)/Ta/Co/Ta structure under both zero and nonzero applied electric field using polarized neutron reflectometry. Application of an electric field across the PMN-PT substrate generates a strain, which rotates the magnetization of the Co layer consistent with the Villari effect. At low magnetic fields (near remanence and coercive field conditions), we find that the depth dependent magnetization profile is non-uniform, under both zero and nonzero applied electric fields. These variations are attributable to the depth dependent strain profile in the Co film, as determined by finite element analysis simulations. *Published by AIP Publishing.*

<https://doi.org/10.1063/1.5037601>

I. INTRODUCTION

Nanomagnetic computing, where information is encoded in the magnetization direction of magnetic nanostructures has the potential to be very energy efficient, is inherently non-volatile,^{1–3} and can lead to novel computing architectures.^{4,5} However, the energy requirements of these devices depend on the magnetization switching mechanism, e.g., external magnetic field,⁶ spin transfer torque,^{7,8} spin Hall effect,^{9,10} voltage controlled magnetic anisotropy^{11,12} or strain induced switching of magnetostrictive nanomagnets.^{13,14} Among these, strain induced magnetization switching is one of the most energy-efficient techniques,^{13,15,16} and is also well suited for non-Boolean computing applications.^{17,18} Strain clocked nanomagnetic memory and logic devices for energy efficient computing have been experimentally demonstrated by a number of groups.^{14,15,19–21} These devices are typically implemented by fabricating magnetostrictive nanomagnets on top of piezoelectric substrates from which voltage induced strain is transferred to produce magnetization rotation. Such strain induced magnetization rotation has been characterized using the Magneto-Optic Kerr Effect (MOKE), Magnetic Force Microscopy (MFM), Photoemission Electron Microscopy (PEEM), magnetoresistance etc.^{14,15,19,22–24} Although MFM, PEEM, and magnetoresistance are excellent at resolving the average and/or near surface magnetization variation, they are unable to resolve the depth dependent magnetization profile. Variation in strain transfer from the piezoelectric substrate to the magnetostrictive layer and therefore, the depth dependent magnetization rotation of such magnetostrictive nanomagnets are yet to be studied in detail. Such variations can have important ramifications in the performance of “straintronic” nanomagnetic devices and can also lead to novel straintronic applications similar to memory devices implemented using

graded media that utilize gradually changing magnetic anisotropy normal to the film.^{25–27} There are other cantilever and thin film based magnetostrictive sensors where this study can prove to be useful.^{28–30}

In this work, we examine the depth dependent magnetization profile in magnetostrictive Co thin films deposited on $(\text{PbMg}_{0.33}\text{Nb}_{0.67})_{1-x}:(\text{PbTiO}_3)_x$ (PMN-PT) (011) substrates with and without electric field induced strain using polarized neutron reflectometry (PNR), which is sensitive to the depth dependent magnetization profile.³¹ We have simulated strain in such a multiferroic heterostructure using finite element analysis to estimate the depth dependent strain transfer profile from the piezoelectric substrate at different depths of the magnetostrictive film, leading to the non-uniformity in the magnetization depth profile. The paper is organized as follows. Section II describes the sample fabrication and characterization methods. Section III presents and analyzes the effect of electric field on the sample coercivity and anisotropy, COMSOL simulation of the strain transfer profile, and the PNR measurements and corresponding models of the depth dependent magnetization profile. Section IV concludes the paper. Additional modeling approaches to the PNR data and data from a second sample to show repeatability are presented in the [supplementary material](#).

II. EXPERIMENTAL METHODS

The PMN-PT substrates $[(\text{PbMg}_{0.33}\text{Nb}_{0.67})_{1-x}:(\text{PbTiO}_3)_x]$; $x = 0.29–0.32$, rhombohedral] used in this work have a (011) orientation with a lateral dimension of $10\text{ mm} \times 10\text{ mm}$ and a thickness of 0.5 mm . The single-side polished substrates have been sourced from MTI Corporation.³² Aluminum (Al) was deposited on the unpolished side of the PMN-PT substrate to be used as the bottom electrode. A 10 nm Ta layer was then deposited on the polished side as an adhesion layer followed by a 60 nm Co layer and 10 nm Ta cap, also used as the top electrode. A schematic of the sample structure is shown in

^{a)}Electronic addresses: alrashidmm@vcu.edu; bhattacharyad@vcu.edu; alexander.grutter@nist.gov; brian.kirby@nist.gov; and jatulasimha@vcu.edu

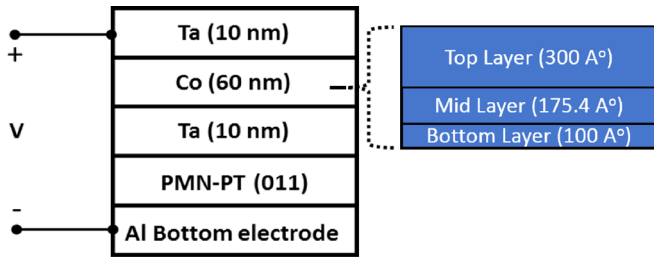


FIG. 1. Sample schematic (the inset shows three different layers used for fitting).

Fig. 1. All the depositions were performed by electron beam evaporation at a base pressure of 3×10^{-6} Torr. Vibrating sample magnetometry (VSM) measurement of the sample was performed at room temperature under zero applied voltage. PNR measurements were performed using the Polarized Beam Reflectometer (PBR) beamline at the NIST Center for Neutron Research. The data were corrected for background, beam footprint, and imperfect beam polarization (unless otherwise mentioned). Model fitting of PNR data allows for determination of the nuclear composition and in-plane vector magnetization depth profiles of thin films and multilayers.³³ Measurements discussed here have been performed at room temperature at multiple magnetic field values, under an applied voltage of either 0 V or 400 V. Model fitting was performed using the ReflID software.³⁴ Finite element analysis simulations were performed using COMSOL to estimate the strain profile in a heterostructure similar to that studied experimentally.

The rationale for choosing 60 nm thickness was the following. While the neutrons are highly penetrating, and interfaces buried under a micron or more of most materials can be studied, the layer thickness one can determine is dependent on the angle and wavelength resolution of the instrument. In our case, we cannot resolve oscillations corresponding to layers thicker than approximately 500 nm.

III. RESULTS AND DISCUSSION

A. Strain effect on the coercive field

Accurately characterizing changes in magnetic properties as a function of electric field can be challenging using

common techniques like VSM or superconducting quantum interference device (SQUID) magnetometry, due to the potential for artifacts arising from the leads. With this in mind, we used PNR measurements taken at a single value of wavevector transfer (Q) to probe the average vector magnetization of the entire sample. Typically, a PNR measurement is carried out over a range of Q , allowing for determination of the depth profiles. Owing to the limited brightness of neutron sources, such measurements can be time consuming, limiting the number of conditions for a given experiment. However, the average magnetization of the entire sample can be approximated by measuring only at very low Q , where the reflectivities are relatively intense (due to proximity to the critical edge), and provide sensitivity to large length scales. Figure 2(a) shows the Q -dependent non-spin-flip ($++$ and $--$) and spin-flip ($+-$ and $-+$) reflectivities at 0 V after magnetically saturating at 700 mT and returning the magnetic field to 1 mT (close to the remanent condition). We chose a Q value of 0.16 nm^{-1} , very near the critical edges, and measured the four reflectivities at that single Q point as functions of magnetic field (H) and voltage (V) after magnetically saturating in -0.7 T , as shown in Fig. 2(b).

The non-spin-flip reflectivities depend on both the nuclear and magnetic composition of a sample. Specifically, the differences in $++$ and $--$ arise from the component of the in-plane sample magnetization parallel to H . Thus, the point where $++$ and $--$ cross corresponds to switching of the parallel component of the magnetization from pointing opposite to H to pointing along H . The spin-flip reflectivities originate from the component of the in-plane sample magnetization perpendicular to H . As such, the peak in the spin-flip scattering shown in Fig. 2(b) corresponds to the maximum angle between the sample magnetization M and applied magnetic field H during reversal. We performed such H -dependent scans at progressively higher voltages, in order to examine the effect of electric field on the magnetic reversal process. We note that the single- Q , H scans shown are not polarization corrected. Since we are not quantitatively estimating magnetization values from these scans (only H -shifts in qualitative features), such corrections are unnecessary. Figure 3(a) shows the non-spin-flip data plotted as spin asymmetry (the difference between $++$ and $--$ divided by the sum). Presented in this way, a change in sign

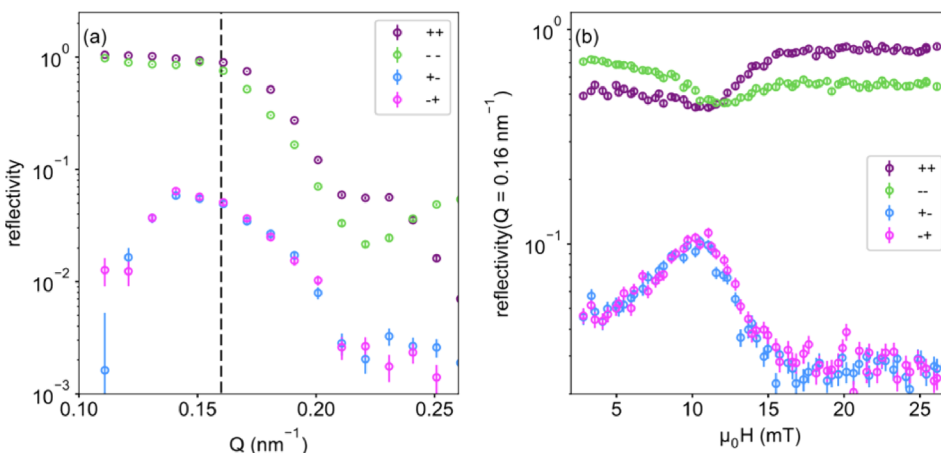


FIG. 2. (a) Low Q PNR data measured at 1 mT and 0 V after positive magnetic saturation. (b) 0 V PNR data as a function of increasing H following negative magnetic saturation. These data correspond to $Q = 0.16 \text{ nm}^{-1}$, indicated by a dashed vertical line in (a). The error bars correspond to ± 1 standard deviation.

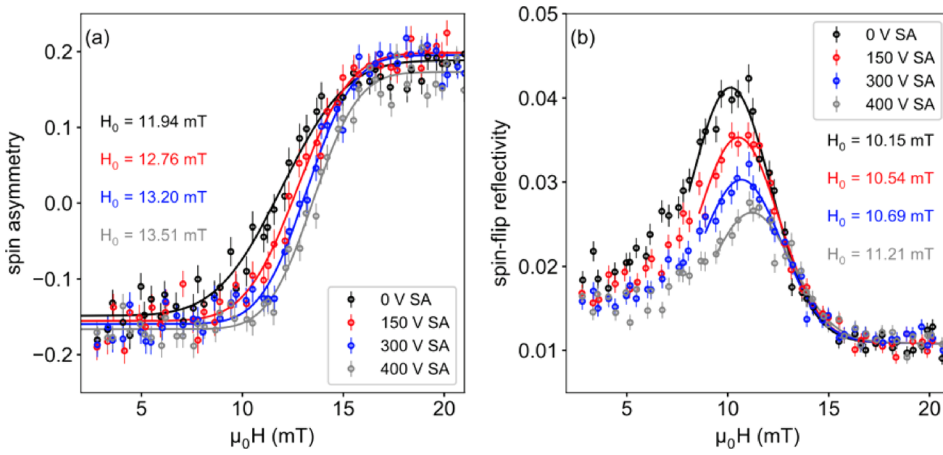


FIG. 3. (a) Spin asymmetry and (b) spin-flip scattering measured at $Q = 0.16 \text{ nm}^{-1}$ as a function of increasing H following negative magnetic saturation. Measurements were repeated at progressively higher applied voltages. The error bars correspond to ± 1 standard deviation.

of the spin asymmetry delineates the transition from M anti-parallel to H to M parallel to H.

The electric field has a clear effect, as the center of the transition H_0 increases progressively by more than 1 mT with the applied voltage. Here, H_0 corresponds to the minimum in magnetization parallel to H, and is estimated by fitting the data to an error function, yielding the values shown in Fig. 3(a) inset. A similar procedure was performed for the spin-flip data, as shown in Fig. 3(b). We expect (and observe) that $+-$ and $-+$ should be identical, therefore the average spin-flip scattering is shown. In this case, H_0 corresponds to the maximum in the perpendicular magnetization and was determined by fitting the data to a Gaussian function, with values shown in Fig. 3(b) inset. Again, the voltage-dependent effects are significant, shifting the peak positions by more than 1 mT. Additionally, the magnitude of the spin-flip peak is observed to progressively decrease with voltage. A VSM measurement of the magnetic hysteresis loop of this sample under zero voltage is shown in Fig. 4. The coercive magnetic field H_c is 12 mT, consistent with transition values shown in Fig. 3, and verifying our interpretation of the PNR signal. The voltage-dependent shifts in magnetization minima parallel to H and corresponding shifts in magnetization maxima perpendicular to H shown in Fig. 3 suggest that the stress anisotropy for a positive applied voltage induces a magnetization “easy axis” (energetically favorable direction) along H, therefore, increasing H_c for the sample.

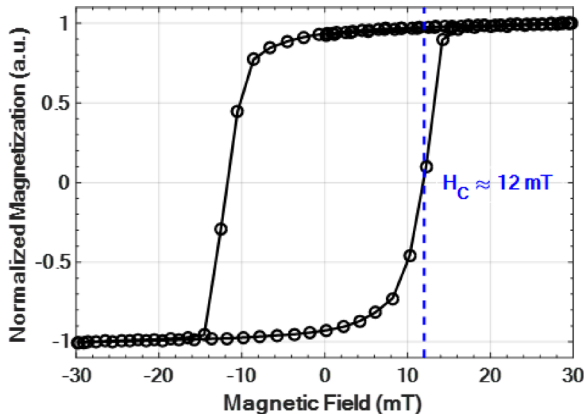


FIG. 4. VSM measurement of the magnetic hysteresis loop at room temperature under zero voltage.

Notably, at all voltages measured, the minima in the spin asymmetry occur at higher H than does the maxima of the spin-flip scattering. This suggests that the magnetization reversal occurs through a combination of coherent rotation and domain nucleation as one would expect in a thin film. We performed MFM at remanence and it appears that the domains are predominantly in-plane (see [supplementary material](#) Sec. III). That the magnitude of the spin-flip peak decreases with voltage is likely a consequence of the increased anisotropy. In a system with high magnetic anisotropy, when the magnetic field is applied along the easy axis, it is energetically costly to rotate or reorient the magnetization through formation of domains with magnetization component perpendicular to the “easy” axis. As a result, with increasing uniaxial-anisotropy, there is a higher likelihood of magnetization reversal through 180° domain formation and motion. An illustration of this is shown in Fig. 5. With increasing applied voltage and therefore stress anisotropy, domains with a perpendicular magnetization component become less energetically favorable, resulting in the observed decrease in the peak spin flip (SF) scattering reflectivities.

B. Depth dependent magnetization rotation

Q-dependent PNR measurements were conducted at 3 different external magnetic fields—positive saturation (at 700 mT), near-remnance (at 1 mT after decreasing the field

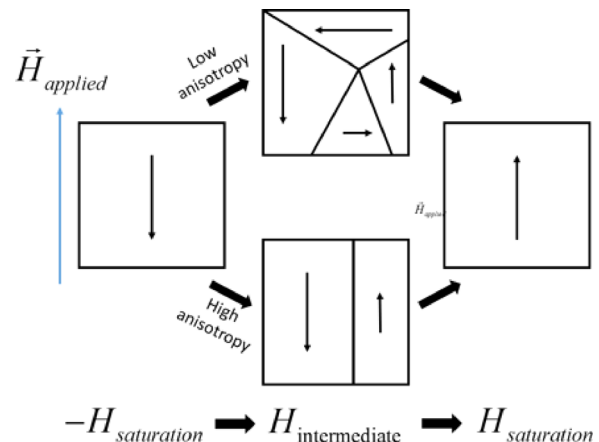


FIG. 5. Magnetization reversal scenarios for different magnitudes of magnetic anisotropy (this illustration is to conceptually explain the reversal mechanism).

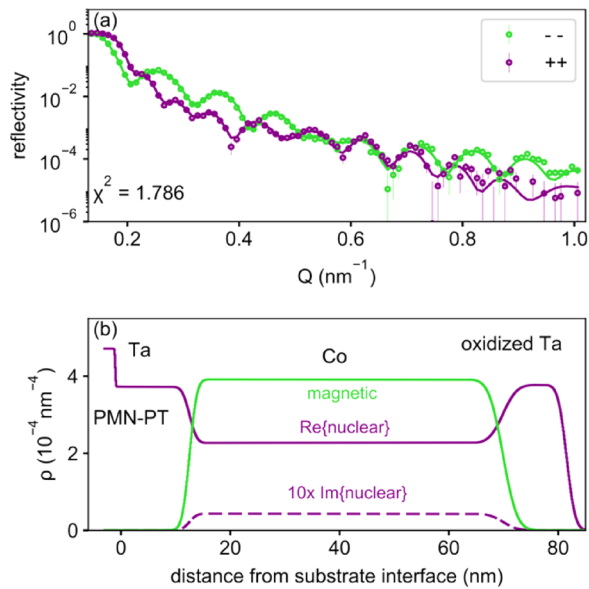


FIG. 6. (a) Fitted PNR data taken at 700 mT and 0 V. (b) Nuclear and magnetic depth profiles used to generate the fits in (a). Note that the magnetic component of ρ is proportional to the magnetization. The error bars correspond to ± 1 standard deviation.

from positive saturation), and near-coercive field (10 mT after increasing the field from negative saturation) in order to determine the depth profiles. Remanence and coercive field measurements were performed at applied voltages of 0 V and 400 V to observe the effects of electric field induced stress on the magnetization profile. The model fitted saturation data is shown in Fig. 6(a). Spin-flip scattering should not be present at saturation, thus only non-spin-flip scattering was measured at this condition. The fit to the data is excellent, and corresponds to the depth profile shown in Fig. 6(b). The profiles are shown in terms of scattering length density

ρ , which has a complex valued nuclear component (corresponding to the nuclear composition) and a magnetic component (proportional to the magnitude of the magnetization vector). The profile is quite simple, with a uniform Co magnetization, and nuclear scattering length densities close to the expected values for all layers. The nuclear profile determined from this fit was used for fits at all other conditions.

At lower magnetic field, we find that the data are inconsistent with a uniform Co magnetization profile. Figure 7(a) shows data taken at 1 mT in 0 V after saturating at 700 mT. Notably, there is significant spin-flip scattering, demonstrating that even at 0 V, anisotropy plays a significant role, as the magnetization relaxes away from the applied magnetic field direction. The fit in Fig. 7(a) corresponds to a profile with depth-independent magnetization magnitude and rotation angle [blue lines Figs. 7(c) and (d)], and does not fit the low- Q spin-flip data well. Figure 7(b) shows the same data as in (a), but the fit is much better, and corresponds to a profile with depth-dependent magnetization magnitude and rotation angle [gray lines Figs. 7(c) and (d)]. Uniform profile fits produce similarly poor results for other measurements at 1 mT and at 10 mT. We found that significant non-uniformity was required to achieve a good fit to the data, but that there were multiple non-uniform models that could provide essentially equivalent fits.

To guide the modeling, we performed simulation of strain transfer in a similar structure using COMSOL. Specifically, we simulated a $\text{Al}_{100\text{nm}}/\text{PZT}_{300\text{nm}}/\text{Ta}_{10\text{nm}}/\text{Co}_{60\text{nm}}/\text{Ta}_{10\text{nm}}$ heterostructure with a lateral dimension of $600 \text{ nm} \times 600 \text{ nm}$ as shown in Fig. 8(a). A uniaxial strain (0.2% tensile strain along x) was applied to the Lead Zirconate Titanate (PZT) layer. The corresponding strain transfer profile through the center of the Co layer as a function of distance from the Ta/Co interface nearest to the piezoelectric layer.

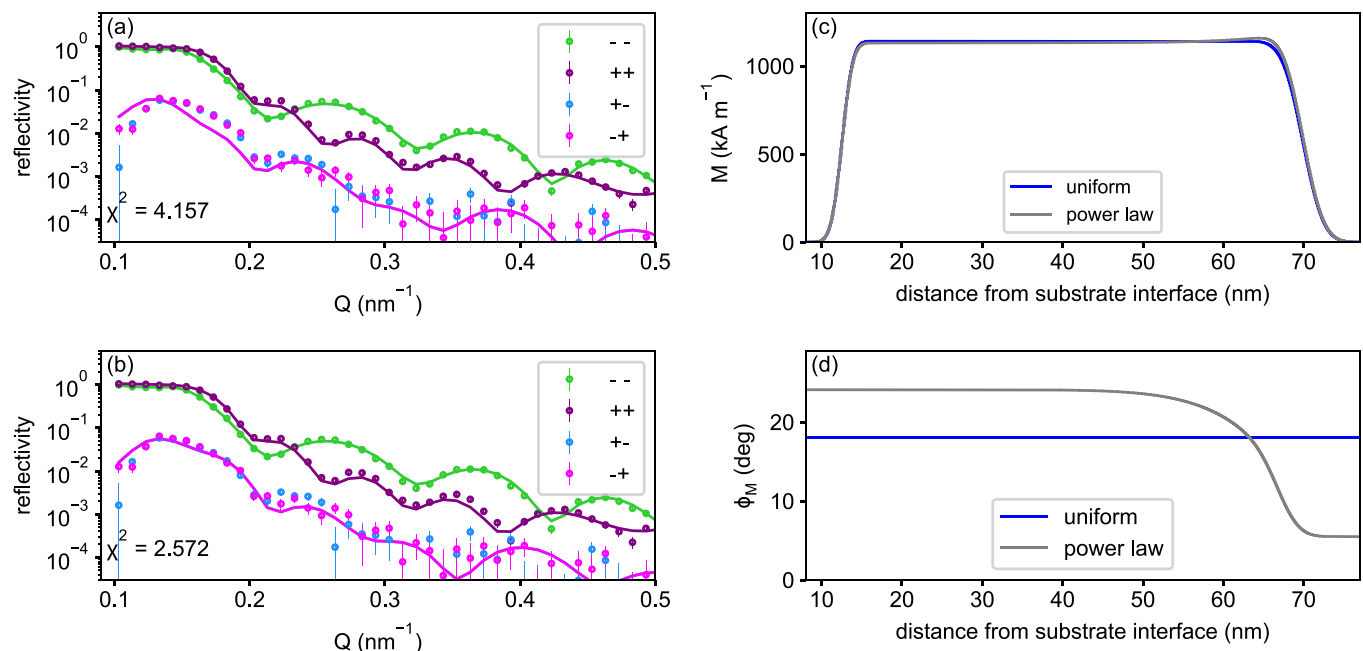


FIG. 7. (a) 1 mT 0 V PNR data with the best fit corresponding to a uniform magnetization profile. (b) Best fit to the same data using a power law model. The error bars correspond to ± 1 standard deviation, (c) magnetization magnitude and (d) magnetization rotation profiles corresponding to the uniform magnetization profile and power law model.

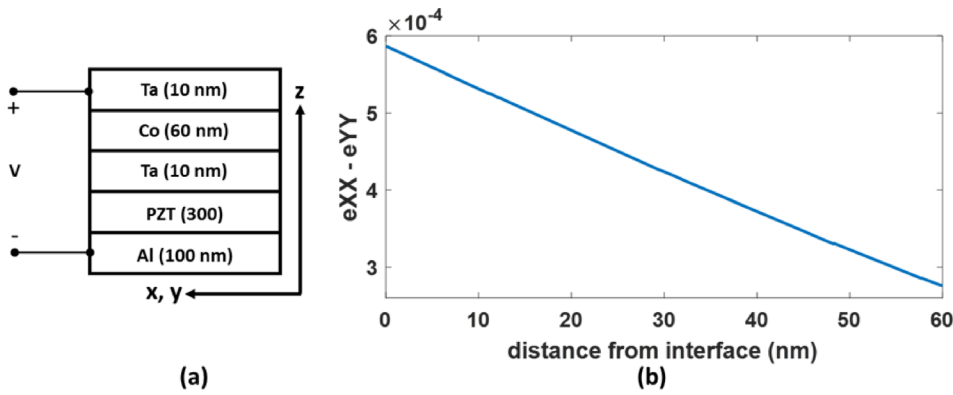


FIG. 8. (a) Structure for the COMSOL model and (b) strain transfer through the center of the Co layer.

The strain transfer changes monotonically with distance. If this strain transfer is responsible for the non-uniformity in the magnetization, it is reasonable to assume that magnetization rotation and magnitude should also change monotonically with depth. Thus, we propose that a monotonic function is appropriate for modeling of the neutron data. For simplicity, we chose a power law, where the endpoint magnetization magnitudes, rotation angles, and the power law exponent were treated as fitting parameters. This scheme results in a much better fit to the data, as shown in Fig. 7(b). The best-fit power law profiles for near-remnance and near-coercivity data are shown in Fig. 9. Figure 9(a) shows the magnitude of the magnetization M , while Fig. 9(b) shows the rotation angle of the magnetization ϕ_M , expressed in terms of the angle between the magnetization vector and the applied magnetic field axis. Note that for the near-remnant conditions, the component of magnetization along the H axis points the same direction as H, while for the near-coercivity conditions, it points opposite. The best-fit parameters are shown in Table I.

The models for the near remanence (1 mT) and near coercive field (10 mT) are discussed in the following sections (subsections 1 and 2).

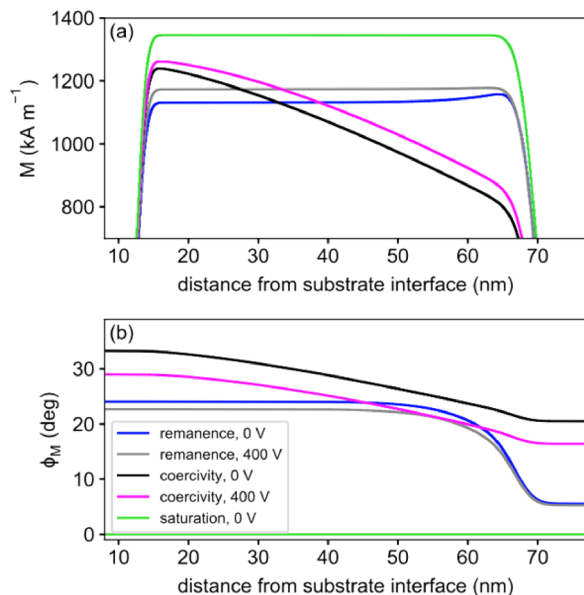


FIG. 9. (a) Magnetization magnitude and (b) magnetization rotation profiles corresponding to the best-fit power law models for the near-remnant and near-coercivity PNR data. The saturation profiles are shown for comparison.

1. Near remanence (1 mT external magnetic field at 0 V and 400 V)

In the 0 V case, although there is no voltage induced stress, a residual stress is present in the Co film from poling of the underlying piezoelectric PMN-PT substrate. The top and bottom layers are rotated by 5.5° and 24.1° (see Table I) from the saturation field direction. Among all the layers, the bottom layer is rotated by the highest amount. This rotation is the result of the residual stress present in the Co film. The effect of this stress is the greatest on the bottom layer (closest to the PMN-PT substrate), which is what the fitting suggests with the bottom layer showing the highest amount of rotation. The Co film is more relaxed (less stress) as we go up, which is also supported by a monotonically decreasing angle of magnetization rotation from the bottom towards the top. When an electrical voltage of 400 V is applied across the sample thickness, the resulting electric field generates a stress in the substrate that is transferred to the Co film. The magnetizations of the Co layers respond to this voltage generated stress by rotating towards the applied magnetic field direction. However, the resulting rotation is very small ($<1^\circ$). The rotation of magnetization towards the saturation field direction due to voltage induced stress matches the observations from Sec. III A. At both 0 V and 400 V, there is a clear difference in the amount of rotation between layers, confirming depth dependent variation in the layer magnetizations.

2. Near coercive field (10 mT external magnetic field at 0 V and 400 V)

The measurements and fitting near the coercive field are quite similar to the measurements at remanence. The difference in measurement conditions is that the sample was first saturated in the negative direction (-700 mT applied magnetic field) which was then increased to 10 mT. Again, similar to the near remanence case, a power law fit is applied. The fitted model and best fit parameters are shown in Fig. 9 and Table I. We can see that both the magnetization orientation and the average magnetization have a depth dependent profile. In the 0 V case, the effect of residual stress is the largest in the bottom layer (deviation of 33.3°) and the smallest in the top layer (deviation of 20.5°). For a small change in magnetic anisotropy, we can expect a larger change in the magnetization near the coercive field compared to the change near remanence (1 mT, decreasing the field from positive

TABLE I. Best-fit parameters for the power law models. The error bars correspond to 2 standard deviations.

Magnetic state	V (V)	Bot M (kA m ⁻¹)	Top M (kA m ⁻¹)	Bot ϕ_M (deg)	Top ϕ_M (deg)	Exponent
Remanent	0	1132 ± 9	1206 ± 31	24.1 ± 0.9	5.5 ± 1.5	8.0 ± 1.7
Remanent	400	1174 ± 9	1187 ± 29	23.0 ± 0.9	5.2 ± 1.5	7.7 ± 1.7
Coercive	0	1248 ± 17	737 ± 22	33.3 ± 1.6	20.5 ± 0.6	1.3 ± 0.1
Coercive	400	1267 ± 16	788 ± 22	29.0 ± 1.4	16.4 ± 0.7	1.5 ± 0.1

saturation). So, the effect of voltage induced stress is expected to be larger near the coercive field compared to remanence. This is exactly what we see from the data in Table I. Here, the bottom layer is rotated by approximately 4° as a result of the voltage induced stress whereas the rotation was approximately 1° in the near remanence case.

Now if we look at the magnetization magnitude profile, we can see that unlike the remanence case, there is clear depth dependence. The apparent magnetization is the highest at the bottom layer and the lowest at the top. This reduction in magnitude can be interpreted in terms of magnetic domains smaller than the coherent projection of the neutron wavepacket on the sample surface, which is between order 1 μm and 100 μm for PBR.^{35,36} At such small length scales, magnetizations pointing in opposite directions effectively cancel, leading to an apparent reduction in magnitude of the magnetization vector. A larger stress in the bottom layer provides a higher anisotropy which possibly results in a magnetic domain distribution where the magnetization directions are more likely to point along the same direction, resulting in a larger apparent magnetization. The top layer experiences a lower stress induced anisotropy possibly allowing the magnetization directions of the domains to have a wider distribution, resulting in a smaller apparent magnetization. So, the layers exhibit a monotonically decreasing apparent magnetization from the interface towards the surface of the Co layer as a result of the similarly decreasing stress induced anisotropy. At 400 V, the voltage induced strain reinforces the magnetic anisotropy along the neutron polarization; we see a corresponding increase in the apparent magnetization of all layers. While this interpretation does correspond to a good fit to the data, we note that other non-uniform models could fit the data as well. However, we can say, with great confidence that while a uniform magnetization profile can fit the data at saturation, at lower field, the profile must be non-uniform.

IV. CONCLUSION

In conclusion, the reflectivity data and the subsequently fitted models clearly show that the voltage induced stress, although very small, has a measurable effect on the magnetization of the Co thin film. The strain induced anisotropy increases the incoherency in the magnetization rotation process as is evident from the “hysteresis-like” measurements performed in Sec. III B. The most important observation in this study is the non-uniform magnetization rotation and average magnetization along the depth of the thin film, a clear indication of depth dependent stress anisotropy in these structures. This study confirms magnetization variation along the thickness of a magnetostrictive thin film which appears

to be related to the relaxation in strain transfer from the piezoelectric substrate to the magnetostrictive layer as we go upwards from the piezoelectric-magnetostrictive heterostructure interface towards the surface of the thin film. This strain variation will possibly be more serious in a patterned 100–200 nm lateral dimension nanostructure even if it is 10 nm thick, which is typically the size for strain mediated nanomagnetic devices. The results presented in this paper are repeatable across samples (the PNR reflectivity data and the corresponding fitted models for a similar but different sample can be found in the [supplementary material](#)).

SUPPLEMENTARY MATERIAL

See [supplementary material](#) for a 3-layer model for the magnetization orientation in the Co layer [that complements the power law fit that was used to explain the polarized neutron reflectometry (PNR) in the main text], for presentation and analysis of data from an additional sample, and for presentation of magnetic force microscopy (MFM) images at remanence.

ACKNOWLEDGMENTS

M.M.A., D.B. and J.A. were funded by NSF Grant Nos. CCF Career 1253370 and ECCS 1609303. The Co films were deposited at the Center for Nanoscale Science and Technology (CNST) Nanofab at NIST, Gaithersburg. Certain commercial equipment is identified in this paper to foster understanding. Such identification does not imply recommendation or endorsement by NIST nor does it imply that the materials or equipment identified are necessarily the best available for the purpose.

¹R. P. Cowburn and M. E. Welland, *Science* **287**, 1466–1468 (2000).

²G. Csaba, A. Imre, G. H. Bernstein, W. Porod, and V. Metlushko, *IEEE Trans. Nanotechnol.* **1**, 209 (2002).

³S. Salahuddin and S. Datta, *Appl. Phys. Lett.* **90**, 093503 (2007).

⁴S. Khasanvis, M. Li, M. Rahman, M. Salehi-Fashami, A. K. Biswas, J. Atulasimha, S. Bandyopadhyay, and C. A. Moritz, *IEEE Trans. Nanotechnol.* **14**, 980 (2015).

⁵S. Khasanvis, M. Li, M. Rahman, A. K. Biswas, M. Salehi-Fashami, J. Atulasimha, S. Bandyopadhyay, and C. A. Moritz, *Computer* **48**, 54 (2015).

⁶M. T. Niemier, G. H. Bernstein, G. Csaba, A. Dingler, X. S. Hu, S. Kurtz, S. Liu, J. Nahas, W. Porod, M. Siddiq, and E. Varga, *J. Phys. Condens. Matter* **23**, 493202 (2011).

⁷J. C. Slonczewski, *J. Magn. Magn. Mater.* **159**, L1 (1996).

⁸D. C. Ralph and M. D. Stiles, *J. Magn. Magn. Mater.* **320**, 1190 (2008).

⁹L. Liu, C.-F. Pai, Y. Li, H. W. Tseng, D. C. Ralph, and R. A. Buhrman, *Science* (80-) **336**, 555 (2012).

¹⁰D. Bhowmik, L. You, and S. Salahuddin, *Nat. Nanotechnol.* **9**, 59 (2014).

¹¹T. Maruyama, Y. Shiota, T. Nozaki, K. Ohta, N. Toda, M. Mizuguchi, A. A. Tulapurkar, T. Shinjo, M. Shiraishi, S. Mizukami, Y. Ando, and Y. Suzuki, *Nat. Nanotechnol.* **4**, 158 (2009).

- ¹²M. Weisheit, S. Fahler, A. Marty, Y. Souche, C. Poinsignon, and D. Givord, *Science* (80-) **315**, 349 (2007).
- ¹³J. Atulasimha and S. Bandyopadhyay, *Appl. Phys. Lett.* **97**, 173105 (2010).
- ¹⁴M. Buzzi, R. V. Chopdekar, J. L. Hockel, A. Bur, T. Wu, N. Pilet, P. Warnicke, G. P. Carman, L. J. Heyderman, and F. Nolting, *Phys. Rev. Lett.* **111**, 027204 (2013).
- ¹⁵N. D'Souza, M. Salehi Fashami, S. Bandyopadhyay, and J. Atulasimha, *Nano Lett.* **16**, 1069 (2016).
- ¹⁶M. M. Al-Rashid, D. Bhattacharya, S. Bandyopadhyay, and J. Atulasimha, *IEEE Trans. Electron Devices* **62**, 2978 (2015).
- ¹⁷S. D. Manasi, M. M. Al-Rashid, J. Atulasimha, S. Bandyopadhyay, and A. R. Trivedi, *IEEE Trans. Electron Devices* **64**, 2842 (2017).
- ¹⁸S. D. Manasi, M. M. Al-Rashid, J. Atulasimha, S. Bandyopadhyay, and A. R. Trivedi, *IEEE Trans. Electron Devices* **64**, 2835 (2017).
- ¹⁹V. Sampath, N. D'Souza, D. Bhattacharya, G. M. Atkinson, S. Bandyopadhyay, and J. Atulasimha, *Nano Lett.* **16**, 5681 (2016).
- ²⁰A. K. Biswas, H. Ahmad, J. Atulasimha, and S. Bandyopadhyay, *Nano Lett.* **17**, 3478 (2017).
- ²¹T. Brintlinger, S. H. Lim, K. H. Baloch, P. Alexander, Y. Qi, J. Barry, J. Melngailis, L. Salamanca-Riba, I. Takeuchi, and J. Cumings, *Nano Lett.* **10**, 1219 (2010).
- ²²M. Salehi-Fashami, M. Al-Rashid, W.-Y. Sun, P. Nordeen, S. Bandyopadhyay, A. C. Chavez, G. P. Carman, and J. Atulasimha, *Nanotechnology* **27**, 43LT01 (2016).
- ²³H. Ahmad, J. Atulasimha, and S. Bandyopadhyay, *Sci. Rep.* **5**, 18264 (2015).
- ²⁴Z. Zhao, M. Jamali, N. D'Souza, D. Zhang, S. Bandyopadhyay, J. Atulasimha, and J. P. Wang, *Appl. Phys. Lett.* **109**, 092403 (2016).
- ²⁵D. Suess, T. Schrefl, S. Fähler, M. Kirschner, G. Hrkac, F. Dorfbauer, and J. Fidler, *Appl. Phys. Lett.* **87**, 012504 (2005).
- ²⁶D. Suess, *Appl. Phys. Lett.* **89**, 113105 (2006).
- ²⁷J. Leiner, B. J. Kirby, M. R. Fitzsimmons, K. Tivakornsasithorn, X. Liu, J. K. Furdyna, and M. Dobrowolska, *J. Magn. Magn. Mater.* **350**, 135 (2014).
- ²⁸A. Tavassolizadeh, T. Meier, K. Rott, G. Reiss, E. Quandt, H. Hölscher, and D. Meyners, *Appl. Phys. Lett.* **102**, 153104 (2013).
- ²⁹G. Buettel, J. Joppich, and U. Hartmann, *Appl. Phys. Lett.* **111**, 232401 (2017).
- ³⁰Y. Hashimoto, N. Yamamoto, T. Kato, D. Oshima, and S. Iwata, *J. Appl. Phys.* **123**, 113903 (2018).
- ³¹G. P. Felcher, R. O. Hilleke, R. K. Crawford, J. Haumann, R. Kleb, and G. Ostrowski, *Rev. Sci. Instrum.* **58**, 609 (1987).
- ³²See <http://www.mtixtl.com/PMNT-011-101005S1.aspx> for more information about PMN-PT substrates.
- ³³C. F. Majkrzak, K. V O'Donovan, and N. F. Berk, *Polarized Neutron Reflectometry in Neutron Scattering from Magnetic Materials* (Elsevier, Amsterdam), pp. 397–471, 2006.
- ³⁴B. J. Kirby, P. A. Kienzle, B. B. Maranville, N. F. Berk, J. Krycka, F. Heinrich, and C. F. Majkrzak, *Curr. Opin. Colloid Interface Sci.* **17**, 44 (2012).
- ³⁵C. F. Majkrzak, C. Metting, B. B. Maranville, J. A. Dura, S. Satija, T. Udovic, and N. F. Berk, *Phys. Rev. A* **89**, 33851 (2014).
- ³⁶L. Fallarino, B. J. Kirby, M. Pancaldi, P. Riego, A. L. Balk, C. W. Miller, P. Vavassori, and A. Berger, *Phys. Rev. B* **95**, 134445 (2017).